

## Measurement of the vector analyzing power $iT_{11}$ in $\pi^+$ - ${}^6\text{Li}$ scattering

S. Ritt, E. T. Boschitz, R. Meier, R. Tacik,\* and M. Wessler

*Kernforschungszentrum Karlsruhe, Institut für Kernphysik and Institut für Experimentelle Kernphysik der Universität Karlsruhe, 7500 Karlsruhe, Federal Republic of Germany*

K. Junker, J. A. Konter, S. Mango, D. Renker, and B. van den Brandt

*Paul Scherrer Institut, 5232 Villigen, Switzerland*

V. Efimovych, A. Kovaljov, and A. Prokofiev  
*Leningrad Nuclear Physics Institute, Leningrad, U.S.S.R.*

R. Mach

*Institute of Nuclear Physics, Československa akademie věd, 25068 Řež, Czechoslovakia*

P. Chaumette, J. Deregel, G. Durand, and J. Fabre

*Département de Physique des Particules Élémentaires, CEN-Saclay, 91191 Gif-sur-Yvette CEDEX, France*

W. Thiel

*Physikalisches Institut, University of Bonn, 5300 Bonn, Federal Republic of Germany*

(Received 16 April 1990)

The vector analyzing power  $iT_{11}$  was measured for  $\pi^+$ - ${}^6\text{Li}$  elastic and inelastic scattering ( $3^+$ , 2.19 MeV) at 100, 134, 164, and 219 MeV, in an angular range between  $40^\circ$  and  $125^\circ$  using a vector polarized  ${}^6\text{LiD}$  target. Sizable spin effects were observed over most of the angular range. The data were compared with a number of theoretical predictions based on different scattering models and nuclear structure input. None of the calculations is able to reproduce the data set; however, it appears that the vector analyzing power  $iT_{11}$  is mostly sensitive to the nuclear wave function chosen. The angular distribution of  $iT_{11}$  in  $\pi^+$ - ${}^6\text{Li}$  elastic and inelastic scattering is discussed in terms of nuclear form factors and elementary  $\pi N$  amplitudes.

### I. INTRODUCTION

In two previous publications<sup>1,2</sup> we reported on pion elastic scattering from polarized  ${}^{15}\text{N}$  at  $T_\pi=164$  MeV. The measured values of the asymmetry  $A_y$  were found to be consistent with zero. This came as a surprise because it was not predicted by any calculation in this mass region, and there is currently no explanation for such a result based on our understanding of the pion nucleus interaction. Instead of continuing our polarization studies with  ${}^{15}\text{N}$  by measuring the dependence of  $A_y$  on pion energy and charge, we proceeded with  ${}^6\text{Li}$  for experimental and theoretical reasons.

Polarized  ${}^6\text{Li}$  became available several years ago in the form of small samples of irradiated  ${}^6\text{LiD}$ ,<sup>3,4</sup> but the task of producing sufficient quantities of this material to be useful for scattering experiments has been hampered by considerable difficulties.<sup>5</sup> Only quite recently a breakthrough occurred,<sup>6</sup> enabling sizable quantities of lithium hydride and lithium deuteride to be produced. The  ${}^6\text{Li}$  polarization (around 50%) is much larger than that which can be obtained for  ${}^{13}\text{C}$ ,  ${}^{14}\text{N}$ , and  ${}^{15}\text{N}$ . Lithium deuteride has the additional advantage that data on  $\pi^+d$  scattering can be obtained simultaneously. The present experiment is the first to make use of a polarized  ${}^6\text{Li}$  target for nuclear research.

From the theoretical point of view  ${}^6\text{Li}$  is an attractive object for nuclear structure and nuclear reaction studies because of the large degree of clustering. The nucleus can be viewed as an  $\alpha$  particle coupled to a neutron-proton pair, and the various techniques which have been developed for solving the three-body problem may be applied in this case. The nuclear structure of  ${}^6\text{Li}$  has been probed extensively in strong, electromagnetic and weak interaction.<sup>7</sup> Within this wealth of data there have been relatively few experiments on the interaction with pions.

Pion elastic and inelastic scattering from  ${}^6\text{Li}$  was measured only at few energies over a limited angular range. Zichy *et al.*<sup>8</sup> measured the elastic and inelastic ( $3^+$ , 2.19 MeV) scattering cross sections at 164 MeV with negative pions. Antonuk *et al.*<sup>9</sup> produced differential cross section data for elastic and inelastic scattering ( $3^+$ , 2.19 MeV) with positive and negative pions at 100, 180, and 240 MeV. Kiziah *et al.*<sup>10</sup> focused their attention on the measurement of the excitation function for the  $\Delta T=1$  transition to the  $0^+,1$  (3.56 MeV) state at a constant momentum transfer ( $q \simeq 109$  MeV/c). In addition to pion elastic and inelastic scattering there have been various measurements in pion induced reactions:  ${}^6\text{Li}(\pi^+,p)$  inclusive (Ref. 11),  ${}^6\text{Li}(\pi^-, \gamma)$  (Ref. 12),  ${}^6\text{Li}(\pi^-, 2n)$  (Ref. 13),  ${}^6\text{Li}(\pi^+, 2p)$  (Ref. 14),  ${}^6\text{Li}(\pi^\pm, \pi^\pm d)$  (Ref. 15), and  ${}^6\text{Li}(\pi^+, {}^3\text{He})$  (Ref. 16).

Most of the theoretical effort has been devoted to elastic and inelastic scattering. Germond<sup>17</sup> studied  $\pi^+{}^6\text{Li}$  scattering in the framework of the Glauber multiple scattering formalism. He used experimental  $\pi\alpha$  and  $\pi N$  scattering amplitudes as well as realistic  $\alpha$ - $n$ - $p$  wave functions<sup>18</sup> as input. His calculation agreed well with the measured differential cross sections at 180 and 240 MeV, but underpredicted the cross sections at 100 MeV. This may indicate that the Glauber approximation is no longer valid at this energy. Germond also predicted the vector analyzing power  $iT_{11}$  at 100, 180, and 240 MeV. It was found to be small except in the vicinity of the minima of the differential cross sections. There, values for  $iT_{11}$  up to 0.5 were predicted.

Eramzhyan *et al.*<sup>19</sup> calculated pion scattering from  ${}^6\text{Li}$  within a momentum space coupled channel formalism. It contained the usual first-order term and the phenomenological  $\rho^2$  term, the parameters of which were determined from  $\pi$ - ${}^{12}\text{C}$  experimental data. A Cluster model wave function<sup>18</sup> and a phenomenological shell model wave function were used for the nuclear states to study nuclear structure effects. Using the cluster model, the elastic scattering cross section could be well reproduced at forward angles, but beyond the first minimum in the cross section serious discrepancies appeared. In this angular region good agreement could be achieved by turning off the second-order ( $\rho^2$ ) term. The inelastic scattering to the  $3^+,0$  (2.19 MeV) state was well described, but there were problems in reproducing the cross sections for the transitions to the  $2^+,0$  (4.31 MeV) and  $0^+,1$  (3.56 MeV) states. In addition to the total and differential cross sections polarization observables were also predicted. It was shown that the vector analyzing power is very sensitive to the nuclear wave function.

There have been two calculations based on the  $\Delta$ -hole model, one by Junker,<sup>20</sup> the other by Nagaoka and Ohta.<sup>21</sup> Junker used the  $\Delta$ -hole formalism of Hirata *et al.*<sup>22</sup> including the  $\Delta$ -spin-orbit potential introduced by Horikawa *et al.*<sup>23</sup> Shell model wave functions were used for  ${}^6\text{Li}$ , with different well parameters for the  $s$ -shell and  $p$ -shell nucleons. For the  $p$ -shell nucleons the empirical wave functions of Donnelly and Walecka<sup>24</sup> were used. Within this model the differential cross sections could be well described. Polarization observables were also calculated. Sizable values of  $iT_{11}$  were predicted, and similar rapid variations with energy and angle were observed as in the calculation by Germond<sup>17</sup> and Eramzhyan *et al.*<sup>19</sup>

Nagaoka and Ohta<sup>21</sup> investigated  $\pi^+{}^6\text{Li}$  scattering on the basis of Watson's multiple scattering theory. A realistic  $\alpha$ - $n$ - $p$  three-body wave function<sup>18</sup> was employed for the ground state and the excited states of  ${}^6\text{Li}$ . The first order optical potential was extended in such a way that the  $\Delta$  dynamics could be described straightforwardly. The in-medium pion-nucleon  $T$  matrix was decomposed into the  $\pi N$  single scattering and the  $\pi N$  scattering mediated by the  $\pi$ -nucleus interaction. The model of Nagaoka and Ohta<sup>21</sup> is equivalent to the model of Hirata *et al.*<sup>22</sup> if the target nucleus is of a closed shell type, and the partial wave mixing due to the Pauli principle is switched off. Many effects were studied in detail by the authors, i.e.,

Fermi corrections,  $\pi N$  background and Coulomb interactions, binding and Pauli corrections, and spreading effects, in particular the importance of the spin-orbit potential. In these model studies reasonable agreement was obtained with the measured differential cross sections at forward angles but considerable discrepancies remained at larger angles. Predictions of the vector analyzing power  $iT_{11}$  in pion elastic scattering were only presented for 100 MeV. This prediction agrees fairly well with those from Germond,<sup>17</sup> Eramzhyan *et al.*,<sup>19</sup> and Junker.<sup>20</sup>

From this brief description of the various calculations it is already clear that the measurement of polarization observables in  $\pi^+{}^6\text{Li}$  scattering is an urgent experimental task. As a first step, the vector analyzing power  $iT_{11}$  could give important information on the degree of  $\alpha$  clustering in the wave functions of the ground state and the excited states in  ${}^6\text{Li}$ . In addition one may be able to constrain certain aspects of the reaction dynamics, e.g., pion absorption as it enters the  $\rho^2$  term in the second-order potential in multiple scattering theories, or the spreading potential in the  $\Delta$ -hole approach. With this purpose in mind we have measured  $iT_{11}$  in pion elastic and inelastic scattering from polarized  ${}^6\text{Li}$  at four energies, i.e., 100, 134, 164, and 219 MeV. The lowest energy was chosen as a bench mark test since rather similar results were predicted from all four types of calculations.

## II. THE EXPERIMENT

### A. Method

The differential cross section  $\sigma^{\text{pol}}$ , for pion scattering from polarized  ${}^6\text{Li}$  (spin 1) can be expressed in terms of  $\sigma^0$ , the cross section for scattering from the unpolarized  ${}^6\text{Li}$ , as

$$\sigma_{\text{pol}} = \sigma^0 (1 + a_{11} iT_{11} + a_{20} T_{20} + a_{21} T_{21} + a_{22} T_{22}), \quad (1)$$

where  $iT_{11}$  and  $T_{20}$ ,  $T_{21}$ ,  $T_{22}$  are the vector and tensor analyzing powers, respectively. Their individual contributions are determined by the coefficients  $a_{11}$ ,  $a_{20}$ ,  $a_{21}$ , and  $a_{22}$ , which are functions of the target vector and tensor polarizations  $p_z$  and  $p_{zz}$  ( $p_{zz} = 2 - \sqrt{4 - 3p_z^2}$ ), and the orientation of the spin quantization axis with respect to the scattering plane, which can be expressed in terms of two angles  $\alpha$  and  $\beta$  (see Ref. 25). With the proper choice of the angles  $\alpha$  and  $\beta$  one can eliminate some coefficients and/or enhance others in order to measure different combinations of the analyzing powers. In the present experiment we chose  $\alpha = 90^\circ$  and  $\beta = 0^\circ$ , i.e., the quantization axis is perpendicular to the scattering plane. In this case, the polarized cross sections are given by

$$\sigma_{\text{pol}}^\pm = \sigma^0 \left[ 1 \pm \sqrt{3} p_z iT_{11} - \frac{\sqrt{3}}{2} p_{zz} \left[ T_{22} + \frac{T_{20}}{\sqrt{6}} \right] \right]. \quad (2)$$

From this equation one obtains

$$iT_{11} = \frac{p_{zz}^-(\sigma^+ - \sigma^0) - p_{zz}^+(\sigma^- - \sigma^0)}{\sqrt{3}(p_{zz}^- p_z^+ + p_{zz}^+ p_z^-) \sigma^0} \quad (3)$$

and the error in  $iT_{11}$

$$(\Delta iT_{11})^2 = \frac{1}{3[(p_{zz}^- p_z^+ + p_{zz}^+ p_z^-) \sigma^0]^2} \times \left[ (p_{zz}^- \Delta \sigma^+)^2 + (p_{zz}^+ \Delta \sigma^-)^2 + \left[ \frac{p_{zz}^+ \sigma^- - p_{zz}^- \sigma^+}{\sigma^0} \Delta \sigma^0 \right]^2 \right]. \quad (3')$$

Note that by definition  $p_{zz}$  is always positive, the  $\pm$  superscript on  $p_{zz}$  in Eq. (3) only refers to the corresponding  $p_z^\pm$ . In the case of  $p_z^+ = p_z^- = p$  and  $p_{zz}^+ = p_{zz}^- = p_{zz}$  these expressions simplify to

$$iT_{11} = \frac{1}{2\sqrt{3}p_z} \left[ \frac{\sigma^+ - \sigma^-}{\sigma^0} \right] \quad (4)$$

and

$$(\Delta iT_{11})^2 = \frac{1}{12(p_z \sigma^0)^2} \left[ (\Delta \sigma^+)^2 + (\Delta \sigma^-)^2 + \left[ \frac{\sigma^+ - \sigma^-}{\sigma^0} \Delta \sigma^0 \right]^2 \right]. \quad (4')$$

In principle, one can measure the composite tensor observable  $\tau_{22} \equiv (T_{22} + T_{20}/\sqrt{6})$  simultaneously with  $iT_{11}$  with this setup ( $\alpha=90^\circ$ ,  $\beta=0^\circ$ ), however, the measurement of  $\tau_{22}$  requires much better counting statistics for the cross sections because  $p_{zz}$  is much smaller than  $p_z$ . In addition, systematic errors in the determination of  $p_z^+$  and  $p_z^-$  enter critically in  $\Delta \tau_{22}$  as discussed in Ref. 26. For this reason, in the present measurement we have focused our attention on the accurate determination of  $iT_{11}$  only.

### B. Experimental procedure

The experimental setup was the same as for our  $\pi^+ - {}^{15}\text{N}$  measurements. The SUSI pion spectrometer at the Paul Scherrer Institute (formerly SIN) in Switzerland was used, together with the polarized target. The  ${}^6\text{LiD}$  target material was prepared at SACLAY, as described in Ref. 6. The target material was polarized by microwave irradiation in a magnetic field of 2.5 T, and the target polarization was determined by comparing the dynamically enhanced polarization NMR signal with the thermal equilibrium signal. Typical polarizing times (for reaching 90% of the maximum values) were 8h. Because of these relative long polarizing times the data taking procedure was similar to the one in the  $\pi^+ - {}^{15}\text{N}$  experiment, namely, instead of reversing the polarity of the target several times while keeping the spectrometer angle fixed, the entire angular distribution was measured before the sign of the target polarization was changed. In this way,  $\sigma^+$ ,  $\sigma^-$ , and  $\sigma^0$  were measured in several cycles. The background in the spectra originating from pion scattering off the walls of the target cell and the  ${}^3\text{He}/{}^4\text{He}$  coolant was measured separately after removing the helium and the target material from the target cell. Data were taken at four pion energies (100, 134, 164, and 219 MeV) in the angular range from  $40^\circ$  to  $125^\circ$ .

## III. DATA REDUCTION

### A. Determination of the cross sections

The polarization observable  $iT_{11}$  is calculated from the cross-section ratios  $\sigma^+/\sigma^0$ ,  $\sigma^-/\sigma^0$  and the target polarizations  $p_z$  and  $p_{zz}$  [Eq. (3)]. In forming the cross-section ratios, the solid angle, the number of target nuclei, and the factor accounting for pion decay in the spectrometer cancel, i.e., only relative cross sections are required. These are obtained from the yield  $y$  in the energy loss spectra, the corresponding number of pions incident on the target,  $n_b$ , the efficiency of the multiwire chambers in the spectrometer,  $\epsilon_{\text{cham}}$ , and the computer efficiency,  $\epsilon_{\text{comp}}$ , according to the equation:

$$\sigma_{\text{rel}} = \frac{y}{n_b \epsilon_{\text{cham}} \epsilon_{\text{comp}}}.$$

In determining the yield of the  $\pi^+ - {}^6\text{Li}$  and  $\pi^+ d$  peaks the background from the metal target cell and helium coolant must be subtracted. This background has been carefully measured in separate experiments. Typical foreground and background subtracted spectra are shown in Fig. 1. Note that the large width of the  $\pi^+ d$  scattering

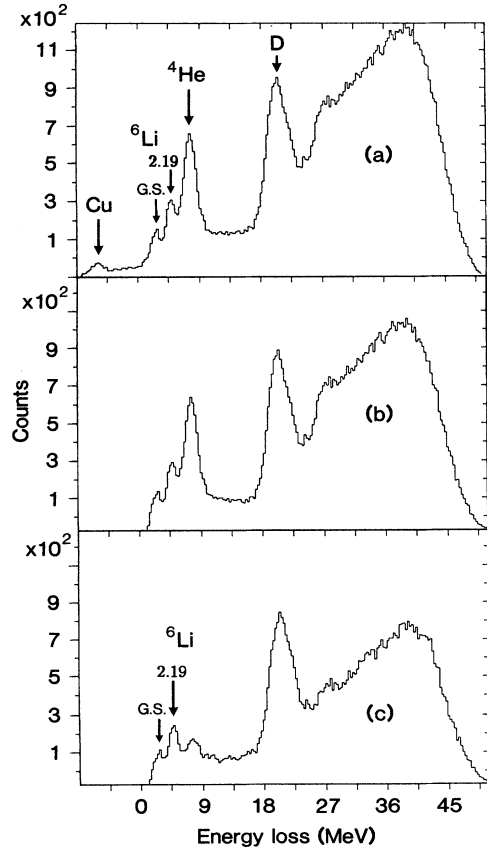


FIG. 1. Typical foreground and background subtracted energy loss spectra for pion scattering from  ${}^6\text{LiD}$  (positive target polarization). (a) Full spectrum. (b) Cu background subtracted. (c) Cu and  ${}^4\text{He}$  background subtracted.

peak is due to the fact that  $\pi^+{}^{-6}\text{Li}$  scattering kinematics was used to calculate these energy-loss spectra. The background subtracted spectra were then subjected to a multiple peak fitting program. From these fits the yields were determined for  $\pi^+{}^{-6}\text{Li}$  scattering to the ground state, the  $3^+,0$  (2.19 MeV) state, and for  $\pi^+d$  scattering. In the spectra higher excited states may be identified, but no effort was made to extract the yields because the underlying background from the pion induced breakup of  ${}^6\text{Li}$  into  ${}^4\text{He}+n+p$  (at 3.70 MeV) and into  ${}^5\text{Li}+n$  (at 5.66 MeV) is not known. On the other hand, the breakup into  ${}^4\text{He}+d$  (at 1.48 MeV), which is located below the  $3^+,0$  (2.19 MeV) peak was estimated from the  $\pi^+{}^{-6}\text{Li}$  spectra in Ref. 9 where an energy resolution of 900 keV allowed a clean separation of the ground state and first excited state peaks.

In Fig. 2 spectra normalized to equal numbers of pions incident on the target are compared for the two polarization states. The solid line corresponds to spectra obtained with positive, the dashed line with negative polarization. As one can see from the difference, there is a large asymmetry in the yields for  $\pi^+{}^{-6}\text{Li}$  scattering to the ground state and first excited state, and also for  $\pi^+d$  scattering.

In spite of the fact that the target thickness was not well known in the present polarization experiment we were able to extract "absolute"  $\pi^+{}^{-6}\text{Li}$  cross sections by normalizing the simultaneously measured relative  $\pi^+d$  cross sections to data from literature<sup>27</sup> (at 100, 134, and 164 MeV interpolated from neighboring energies). The fair agreement between our normalized  ${}^6\text{Li}$  cross sections at 164 MeV and the previous measurement<sup>8</sup> (Fig. 3), as well as between our 100 MeV data and a previous measurement,<sup>9</sup> as shown in Fig. 12 in Sec. VC, provides a measure of confidence of our data extraction procedure. In addition, new data at 134 and 219 MeV are produced for comparison with theoretical predictions. At this point, a word of caution for the theorists may be in order.

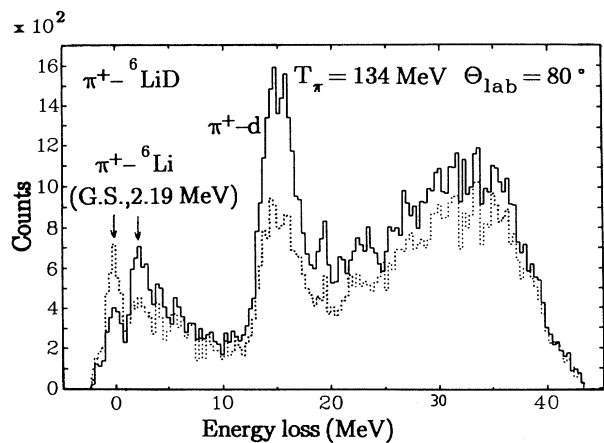


FIG. 2. Comparison of corresponding energy loss spectra for positive (solid line) and negative (dotted line) target polarization. Note the large positive asymmetry for  $\pi^+d$  and  $\pi^+{}^{-6}\text{Li}$  ( $3^+, 2.19$  MeV) scattering and the negative asymmetry for  $\pi^+{}^{-6}\text{Li}$  (ground state) scattering.

A critical examination of the data presented by Antonuk *et al.*<sup>9</sup> shows considerable inconsistencies. The large discrepancies between the  $\pi^+$  and  $\pi^-$  elastic and inelastic cross sections in some angular regions is hard to understand. Similarly, there may also be errors in the elastic and inelastic cross section data of Zichy.<sup>8</sup> For example, due to poor energy resolution and insufficient statistical accuracy in the measurements, the cross section extracted for the  $(0^+, 1)$ , 3.56 MeV state was later found to be incorrect. Therefore the existing data on differential cross sections should be checked and measurements extended to other energies.

### B. Determination of the target polarization

The polarization of  ${}^6\text{Li}$  (as well as that of D) has been determined by NMR techniques, from the ratios of the dynamically enhanced (DYN) polarization signals to the thermal equilibrium (TE) polarization signal at 2.17 K. Figure 4 shows a TE signal, corresponding to  $p=0.23\%$  and a  ${}^6\text{Li}$  DYN signal, corresponding to  $p \approx 50\%$ . Deuteron signals, not shown, were of comparable quality. While the  ${}^6\text{Li}$  polarization was monitored continuously during the experiment, the deuteron polarization was measured only in regular intervals, and it was found to be consistent with the values predicted from equal spin tem-

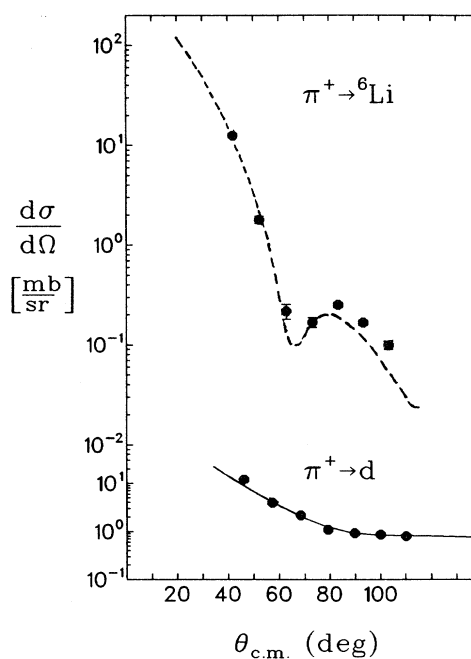


FIG. 3. Consistency test for extracting cross sections at 164 MeV from the present polarization experiment. In the lower half of this figure "relative"  $\pi^+d$  cross sections from this experiment (full circles) are normalized to  $\pi^+d$  cross sections from Ref. 27, interpolated to 164 MeV (solid line). Applying this normalization factor "absolute"  $\pi^+{}^{-6}\text{Li}$  cross sections (full circles) are obtained, and compared with  $\pi^+{}^{-6}\text{Li}$  data from Ref. 8 (dashed line).

perature theory.

The NMR system used in this experiment was briefly described in Ref. 2; a detailed technical report is forthcoming.<sup>28</sup> A strongly damped series resonance circuit was used for the measurement of the  ${}^6\text{Li}$  and D polarization in place of the high- $Q$  parallel resonance circuit used for  ${}^{15}\text{N}$  in  ${}^{15}\text{NH}_3$ . Corrections for the dispersion term of the magnetic susceptibility were obtained from a mathematical simulation of the  $Q$ -meter circuit, illustrated schematically in Fig. 5. The ratio of the NMR signal

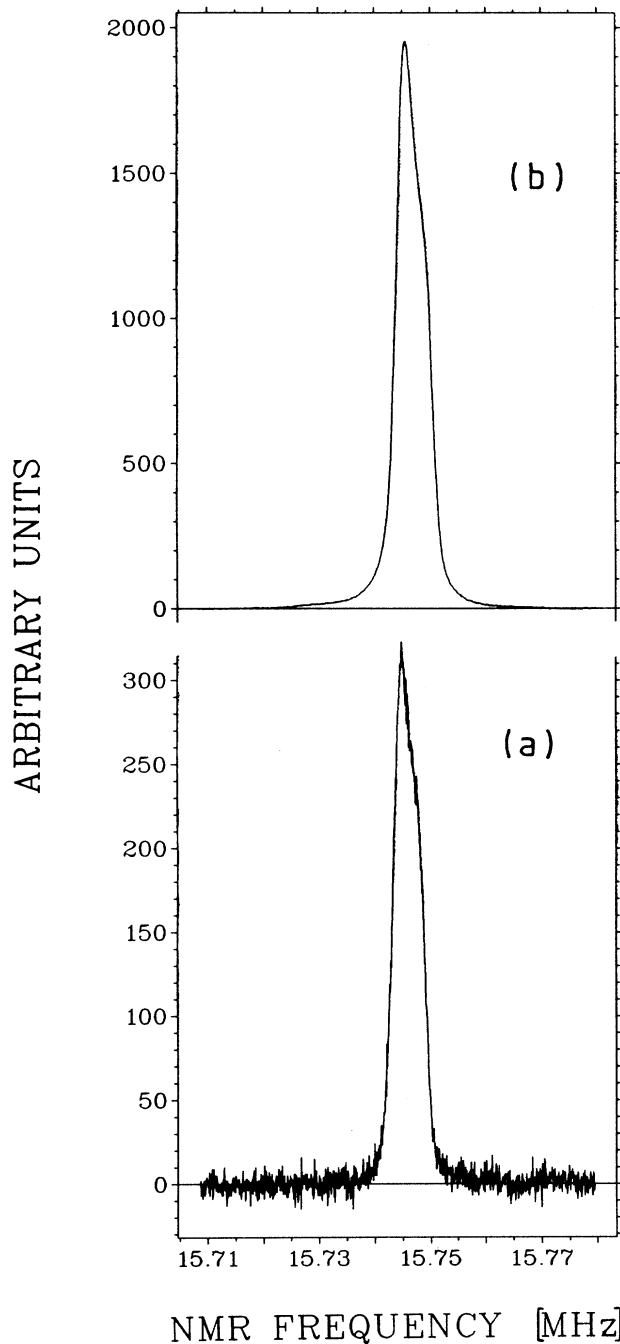


FIG. 4. Typical thermal equilibrium (a) and dynamically enhanced (b) NMR signals for polarized  ${}^6\text{Li}$ .

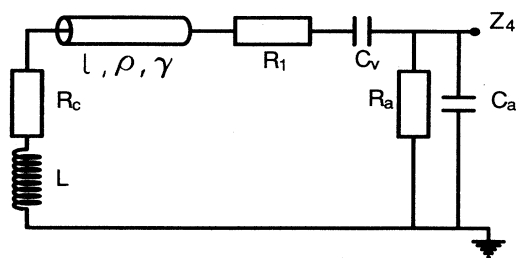


FIG. 5. Schematic diagram of the  $Q$ -meter circuit used to calculate the corrections to the measured target polarization.

amplitude to the corresponding voltage level was calculated from the following equations:

$$S(\omega, X'') = \frac{|Z_4(\omega, X'')| - |Z_4(\omega, 0)|}{|Z_4(\omega_0, 0)|}, \quad (5)$$

$$Z_4(\omega, X'') = (1/Z_3 + 1/R_a + i\omega C_v)^{-1}, \quad (6)$$

$$Z_3 = \frac{Z_2 + \rho \tanh(\gamma l)}{1 + Z_2 \tanh(\gamma l)/\rho} + R_1 + \frac{1}{i\omega C_v}, \quad (7)$$

$$Z_2 = i\omega L(1 + G(X' - iX'')) + R_c, \quad (8)$$

where  $R_a$  is the input resistance of the rf amplifier,  $L$  is the inductance of the coil,  $R_c$  is the resistance of the coil,  $C_v$  is the tuning capacitance,  $R_1$  is the damping resistor,  $\gamma$  is the propagation constant of the cable,  $l$  is the cable length,  $\rho$  is the wave resistance,  $X''$  is the absorption, normalized to a maximum of 1,  $X'$  is the dispersion calculated from the Kronig-Kramers equation,  $G$  is the filling factor of the coil, and  $\omega_0$  is the middle value of frequency sweep.

The  $Q$ -meter parameters were measured at room temperature. Since they may change slightly at low temperatures, they were checked by fitting the measured resonance curve  $|Z_4| = F(\omega)$  in a frequency range of about 10 MHz. The ratio of the signal amplitude to the detector voltage level,  $E_s$ , was known from  $Q$ -meter measurements, and we were able to determine the filling factor  $G$  by iteration according to Eq. (5).

We assumed the absorption to have a Gaussian line shape:

$$X = E/E_s e^{-(\omega - \omega_0)^2/\sigma^2},$$

where  $E$  is the "true" enhancement of the dynamical signal over the thermal equilibrium signal. The corrections  $C$  to the measured polarization value  $p_0$  were calculated for different values  $E$  and  $E_s$ , according to the expression

$$C = \frac{\int_{\omega_1}^{\omega_2} S(\omega, E/E_s e^{-(\omega - \omega_0)^2/\sigma^2}) d\omega}{E \int_{\omega_1}^{\omega_2} S(\omega, 1/E_s e^{-(\omega - \omega_0)^2/\sigma^2}) d\omega} - 1,$$

where  $\omega_1$  and  $\omega_2$  determine the frequency range sampled. The corrected polarization  $p$  is obtained from

$$p = p_0 / (1 + C),$$

$C$  was found to be 0.04 for positive, and  $-0.06$  for negative polarizations. With these corrections the maximum lithium polarizations amounted to  $p^+ = 50.4\%$  and  $p^- = 48.2\%$ , while the corresponding deuteron polarizations were  $p^+ = 52.2\%$  and  $p^- = 49.9\%$ . We estimated the error  $\Delta p/p$  to be  $\pm 5\%$ .

### C. Determination of $iT_{11}$

The determination of  $iT_{11}$  from the measured cross sections and the target polarizations followed the procedures described in an earlier publication.<sup>26</sup> The “fitting method” makes use of Eq. (1). Since  $p_{zz}$  can be approximated by  $p_{zz} \approx \frac{3}{4}p_z^2$ . Equation (1) becomes a quadratic equation in  $p_z$ , i.e.,

$$\sigma^{\text{pol}}(p_z) = A + Bp_z + Cp_z^2$$

where  $A = \sigma^0$ ,  $B = \sqrt{3}\sigma^0 iT_{11}$  and  $C = (3\sqrt{3}/8)\sigma^0\tau_{22}$ . Fitting this function to the measured cross sections for different target polarizations at a given scattering angle and pion energy, the coefficients  $A$ ,  $B$ ,  $C$  can be determined. From  $A$  and  $B$  the vector analyzing power  $iT_{11}$  and the error  $\Delta iT_{11}$  can be calculated:

$$iT_{11} = \frac{B}{\sqrt{3}A}, \quad \Delta iT_{11} = iT_{11} \left[ \left( \frac{\Delta A}{A} \right)^2 + \left( \frac{\Delta B}{B} \right)^2 \right]^{1/2}$$

With this method a mean value for  $iT_{11}$  is obtained, weighting the separate measurements according to their individual errors.

The “matrix method” displays values for  $iT_{11}$  calculated from each pair of relative cross sections  $\sigma^+/\sigma^0$  and  $\sigma^-/\sigma^0$  in the form of a matrix. Comparing the average  $iT_{11}$  value for rows and columns one can recognize systematic errors.

In the “summation method” for each target polarization all spectra taken at each angle are added up and the sum-yield is determined. From this yield, the integrated number of incident pions, and the average computer and chamber efficiencies, the cross section is calculated. The analyzing power  $iT_{11}$  is then determined from the  $\sigma^+$ ,  $\sigma^-$ , and  $\sigma^0$  cross sections and the beam weighted averages of the positive and negative target polarizations, respectively. With this method, the yields are obtained with different statistics providing an independent test of the fitting of the spectra.

The target material  ${}^6\text{LiD}$  has the advantage that the analyzing power  $iT_{11}$  can be measured for  $\pi^+{}^6\text{Li}$  and  $\pi^+d$  scattering simultaneously, providing an additional consistency test. In Fig. 6 we compare  $\pi^+d$  data from this experiment with recent measurements from our group,<sup>26</sup> where both a different scattering technique ( $\pi^+d$  coincidence method) and a different target material (deuterated propandiol) were used. The curve is the result of a  $\pi^+d$  calculation of Ferreira and Dosch<sup>29</sup> within their  $N\Delta$  model. For this calculation all existing  $\pi^+d$   $\sigma(\theta)$  and  $iT_{11}(\theta)$  data between 117 and 325 MeV have been fitted for each energy individually and a surprisingly consistent variation of the fitting parameters has been obtained.

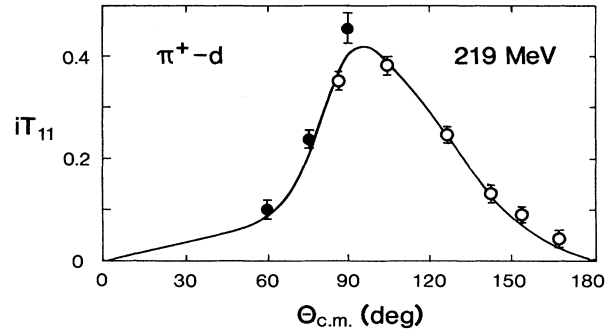


FIG. 6. Comparison of the vector analyzing power  $iT_{11}$  for  $\pi^+d$  scattering from this experiment (solid circles), with corresponding data from an earlier experiment (Ref. 26; open circles). The solid line is the result of a calculation of Ferreira and Dosch (Ref. 29; see text).

## IV. OUTLINE OF THE THEORETICAL CALCULATIONS

A comparison has been made of our experimental data with the predictions from the isobar-hole and coupled channel models.<sup>22,30</sup> Here we summarize the formalism and specify the nuclear structure input.

### A. Isobar-hole model

The model is particularly designed for applications in the vicinity of the  $\Delta$ -resonance, which occurs in the pion-nucleon  $P_{33}$  wave at  $T_\pi \approx 190$  MeV. For pion energies above and below the resonance it corresponds to a conventional first-order optical potential. Here, the dominant mode of pion-nucleus interaction is the excitation of a nucleon to a  $\Delta$  resonance. This process leaves a hole in the nuclear state under consideration. Then the pion-nucleus scattering  $T$  matrix is given as

$$T = T_0 + F \frac{1}{D(E - H_\Delta) - W_\pi - W_p - W_{sp}} F^+, \quad (9)$$

where  $T_0$  receives a contribution from nonresonant  $\pi N$  amplitudes only. At energies well below the resonance a repulsive  $s$ -wave term proportional to nuclear density squared is to be added to  $T_0$ . The strength of the term is a free parameter of the model. The denominator in Eq. (9) represents an isobar Hamiltonian in the space consisting of the  $\Delta$  resonance and  $(A - 1)$  nucleons. Further,  $W_\pi$  stands for a self-energy term associated with pion rescattering and  $W_p$  represents the Pauli-principle correction. Its meaning is simple. Such an isobar decay is forbidden when it leads to an already occupied nucleonic state.

An important assumption is inherent in the isobar-hole model. Namely, the  $\pi N \rightarrow \Delta$  vertex function in the nuclear medium is assumed to be the same as in free space, however, corrected for the right momentum dependence corresponding to the transformation to the  $\pi$ -nucleus center-of-mass system. Then, providing that the nuclear wave function and shell model potential are known, one can calculate  $H_\Delta$ ,  $W_\pi$ ,  $W_p$ , and  $F$ . The latter symbol stands for a transition operator connecting a  $\Delta$ -hole state

to a low-lying nuclear excited (or ground) state plus a noninteracting pion.

On the other hand, it is very difficult to calculate the  $\Delta$ -hole coupling either to higher nuclear excited states or to multi-isobar configurations. Such contributions, denoted as  $W_{sp}$  in Eq. (9) are usually taken into account in a phenomenological way. We introduced the spreading potential  $W_{sp}$  as

$$W_{sp} = W_0 \frac{\rho(r)}{\rho(0)} + 2W_0^{LS} V_{LS}(r) \mathbf{L}_\Delta \cdot \mathbf{S}_\Delta, \quad (10)$$

where  $\rho(r)$  is the nuclear density and  $V_{LS}(r)$  was assumed to have a Gaussian shape. The complex strength parameters  $W_0$  and  $W_0^{LS}$  were adjusted to reproduce total and elastic  $\pi$ - ${}^6\text{Li}$  differential cross sections.

In the case of the  ${}^6\text{Li}$  nucleus, where the nucleon  $p$  shell is partially filled, the Pauli blocking term  $W_p$  has a rather complicated structure. The operator couples the core and valence particle spaces. This mixing was neglected in our calculations and  $W_p$  was assumed to be diagonal in the  $p$ -shell states, and  $p$ -state independent.

The nuclear wave function

$$\Psi_{J^+T} = \Psi_\alpha \sum_i a_i \phi_i^{J^+T} \quad (11)$$

was constructed within the harmonic oscillator model. Here,  $\phi_i^{J^+T}$  denotes the valence nucleon wave function and  $i$  labels the  $(1p)^2$  configurations. In the case of the  ${}^6\text{Li}$  ground state, we used the admixture coefficients  $a_i$  as obtained by Donnelly and Walecka<sup>24</sup> and also their value of the oscillator parameter  $b = 2.03$  fm for  $p$ -shell nucleons. Further,  $\Psi_\alpha$  is the  $\alpha$ -cluster wave function approximated here by the  $(0s)^4$  configuration. A different value of the oscillator parameter was chosen for the  $s$ -shell nucleons. The value  $b = 1.65$  fm allows one to reproduce the longitudinal  $e$ - ${}^6\text{Li}$  elastic form factor at least in the region of small transferred momenta.

The ansatz (11) was used also in the case of the  $(3^+, 0)$  excited state. However, the valence nucleons were allowed to occupy higher oscillator states up to  $1f$ - $3p$  configurations. The corresponding admixture coefficients were obtained by fitting the experimental transition  $C2$  form factor in inelastic  $e$ - ${}^6\text{Li}$  scattering<sup>32,33</sup> assuming the normalization of the  $\Psi_{3^+,0}$  wave function also to be a free parameter. The resulting values of admixture coefficients

TABLE I. Admixture coefficients  $a_i$  in the  $\Psi_{3^+,0}$  wave function.

$i$	Configurations of valence nucleons						$a_i$
	$n$	$j$	$l$	$n$	$j$	$l$	
1	1	$\frac{1}{2}$	1	1	$\frac{5}{2}$	3	-0.129 95
2	1	$\frac{1}{2}$	1	1	$\frac{7}{2}$	3	-0.389 84
3	1	$\frac{3}{2}$	1	1	$\frac{3}{2}$	1	0.165 40
4	1	$\frac{3}{2}$	1	2	$\frac{3}{2}$	1	0.519 79
5	1	$\frac{3}{2}$	1	3	$\frac{3}{2}$	1	0.233 91
6	1	$\frac{3}{2}$	1	1	$\frac{5}{2}$	3	-0.389 84
7	1	$\frac{3}{2}$	1	1	$\frac{7}{2}$	3	-0.571 76

are given in Table I. The norm of the  $\Psi_{3^+,0}$  wave function turned out to be  $N^2 = |\langle \Psi_{3^+,0} | \Psi_{3^+,0} \rangle|^2 = 5.448$ . In what follows the model will be referred to as ‘‘shell model  $J$ .’’

### B. Coupled-channel model

Within the momentum-space coupled-channel formalism, the pion-nucleus scattering matrix  $T(E)$  is given as a solution of

$$T(E) = V(E) + V(E)PG(E)T(E). \quad (12)$$

Here,  $G(E)$  is the pion-nucleus Green’s function,  $V(E)$  stands for a potential matrix and  $P$  is a projection operator, which projects onto the group of nuclear states being taken explicitly into account. The potential matrix

$$V(E) = V^{(1)}(E) + V^{(2)}(E) \quad (13)$$

can be split into a first-order term  $V^{(1)}(E)$  and a phenomenological term  $V^{(2)}(E)$ , which accounts for pion absorption and higher-order processes.

Using the impulse approximation, we can express the matrix elements of the potential  $V^{(1)}(E)$  in terms of the elementary  $\pi N$  amplitude  $t(E)$  and nuclear form factors.<sup>19</sup> The meaning of impulse approximation is the following: the amplitude  $t(E)$  is assumed to be the same in nuclear medium as in the free space. Therefore the coupled-channel model in its present form does not allow one to introduce medium modifications to the intermediate isobar propagation and in this sense is more restrictive than the isobar-hole model.

On the other hand, the nuclear structure information enters the matrix element of  $V^{(1)}(E)$  via nuclear reduced matrix elements

$$M_{nm}^{JLST}(q) = A (J_n T_n || | \tau^{(T)} j_L(qr) [Y_L \otimes \sigma^{(S)}]_J || | J_m T_m), \quad (14)$$

where, e.g.,  $\sigma^{(S)} = 1$  for  $S = 0$  and  $\sigma^{(S)} = \sigma$  for  $S = 1$ . Further,  $J_m (T_m)$  is the spin (isospin) of the nuclear state  $m$ . The matrix elements (14) can often be deduced from electron scattering experiments. Therefore, it is easier to work with a reliable nuclear structure input within the coupled-channel model than in the isobar-hole model, which operates directly with nuclear wave functions.

Since the coupled-channel model was applied to the pion scattering from  $p$ -shell nuclei<sup>36</sup> and, in particular, to  $\pi$ - ${}^6\text{Li}$  scattering,<sup>19</sup> we only summarize its essential features here.

(i) The second order potential  $V^{(2)}(E)$  is assumed to be diagonal in nuclear states and to be a scalar-isoscalar quantity. The functional form of its matrix element was chosen as the Fourier transform of the nuclear density squared and the energy dependence of the second-order potential was obtained by fitting the  $\pi$ - ${}^{12}\text{C}$  scattering data. For further details we refer to Ref. 30.

(ii) The nuclear Fermi motion is treated here in the factorization approximation: Instead of averaging over the nucleonic motion, we use fixed optimal values of nucleon momenta. This is the reason why the spin-flip part of the first-order potential is build up solely from the spin-flip part of the  $\pi N$  amplitude.

(iii) The separable potential model was used to define the off-energy-shell extrapolation of  $\pi N$  amplitudes. The separable  $\pi N$  potential here plays much the same role as the  $\pi N \rightarrow \Delta$  vertex function in the isobar-hole model.

Two different models of nuclear structure were used in our calculations. The first one is also based on the ansatz (11) and the work by Donnelly and Walecka.<sup>24</sup> A slightly more complicated parametrization of the  $\alpha$ -cluster wave function  $\Psi_\alpha$  was used here, which provides a better fit to the experimental longitudinal  $e$ - ${}^6\text{Li}$  elastic form factor in the region  $0 < q < 3 \text{ fm}^{-1}$ . In the case of the  $(3^+, 0)$  excited state, only the  $(1p)^2$  configuration was assumed. However, the transition reduced matrix element  $M_{(3^+, 0)(1^+, 0)}^{2200}(q)$  [see Eq. (14)] was replaced by an empirical expression deduced from inelastic electron scattering experiments.<sup>32,33</sup> A reasonable fit to the measured longitudinal form factor was obtained in the region  $0 \leq q \leq 2.5 \text{ fm}^{-1}$  by using the parametrization

$$|F_L(q)|^2 = (aq)^4 [1 - (cq)^2 + (dq)^4] \exp(-\frac{5}{12} b^2 q^2). \quad (15)$$

Here,  $a^2 = 0.375 \text{ fm}^2$ ,  $c^2 = 0.220 \text{ fm}^2$ ,  $d^2 = 0.313 \text{ fm}^2$  and  $b = 2.03 \text{ fm}$ . Parameter  $a$  was chosen to reproduce the reduced transition coefficient  $B(C2, 0)$  measured by Yen *et al.*<sup>32</sup> In what follows this model will be referred to as the “shell model  $M$ .”

The  $\alpha$ - $N$ - $N$  cluster model by Krasnopol'sky *et al.*<sup>18</sup> was also used in our coupled-channel calculations. The nuclear wave functions are obtained within this model by variational techniques using realistic  $V_{NN}$  and  $V_{\alpha N}$  potentials as dynamical input. Pauli principle effects are taken into account to some extent. This model will be referred to as the “cluster model.”

### C. Nuclear structure input

The polarization observables were shown<sup>19</sup> to depend strongly on the underlying nuclear structure input. We arrive here at the same conclusions. To make the differences between various nuclear wave functions used in our calculations more evident, we discuss here the extent to which they account for the properties of  ${}^6\text{Li}$  as observed in electromagnetic processes. In Table II we give the ground-state quadrupole ( $Q$ ) and magnetic ( $\mu$ ) moments and the reduced transition probability  $B(C2, 0)$ .

It can be concluded that the cluster model reproduces

TABLE II. Predictions of several nuclear models for static properties of  ${}^6\text{Li}$  in comparison with experiment.

	$Q$ (mb)	$\mu$ (nm)	$B(C2, 0)$ (fm)
Cluster model	2.4	0.832	
Shell model $J$	-0.807	0.8228	20.24
Shell model $M$	-0.807	0.8228	21.8
Experiment	$-0.80 \pm 0.08$	0.82201	$21.8 \pm 0.8$
	(Ref. 7)	(Ref. 7)	(Ref. 32)

the ground-state magnetic moment quite well, while the quadrupole moment turns out to be wrong as far as its magnitude and sign concerns. The shell model  $J$  and  $M$  yield the same value of  $\mu$  and  $Q$  as the underlying Donnelly and Walecka model<sup>24</sup> in reasonable accordance with experiment. By its construction, the shell model  $M$  reproduces the experimental  $B(C2, 0)$  value.

This value was not included in the list of fitting parameters in obtaining the admixture coefficients in Table I. Nevertheless, the shell model  $J$  yields  $B(C2, 0)$  in a reasonable agreement with the experiment.

Further, the ground-state longitudinal form factor is shown in Fig. 7. The shell model  $J$  and  $M$  predict smaller  $F(C2, q)$  in the interval  $0 \leq q \leq 2.2 \text{ fm}^{-1}$  than the cluster model. In this interval, the sign of  $F(C2, q)$  turns out to be positive in the cluster model and negative in the shell model  $J$  and  $M$ . The cluster model yields the resulting longitudinal form factor  $|F_L(q)| \equiv [F(C0, q)^2 + F(C2, q)^2]^{1/2}$  in very good agreement with the experiment in the whole interval of transferred momenta considered ( $0 \leq q \leq 3.6 \text{ fm}^{-1}$ ), while the parametrization chosen in the shell model  $J$  and  $M$  reproduces the data in the intervals  $0 \leq q \leq 2.1 \text{ fm}^{-1}$  and  $0 \leq q \leq 2.6 \text{ fm}^{-1}$ , respectively.

Neither the cluster model nor the shell model  $J$  and  $M$  (i.e., the Donnelly and Walecka wave functions) reproduce the ground-state transverse form factor satisfactorily. This can be seen in Fig. 8. The cluster model overestimates the experimental data at small  $q$  and the dip in  $F_T^2(q)$  occurs at larger  $q$  than in the experiment. The wave function by Donnelly and Walecka reproduces the

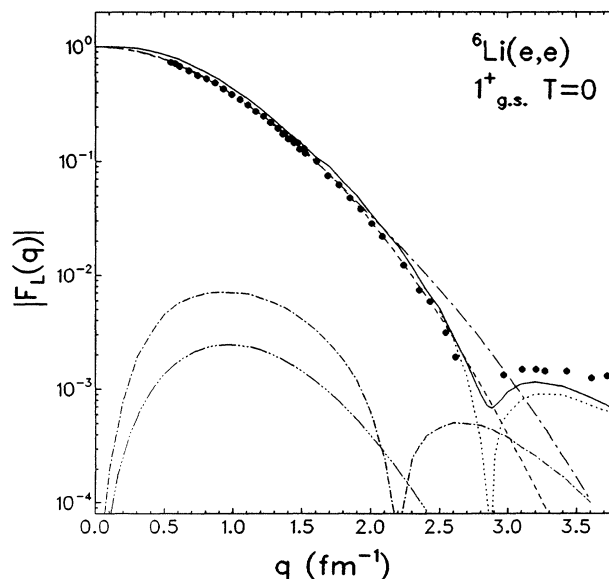


FIG. 7. Longitudinal form factor in elastic scattering by  ${}^6\text{Li}$ . Cluster model (Ref. 18); C0 form factor (dotted line), C2 form factor (dash-dotted line) and resulting  $|F_L(q)|$  (solid line). Shell model (Ref. 24): C2 form factor (triple-dot-dashed line). Parametrization of  $|F_L(q)|$  by Junker (long-dashed-dotted line) and Mach (dashed line). Experimental data are from Refs. 31 and 34.

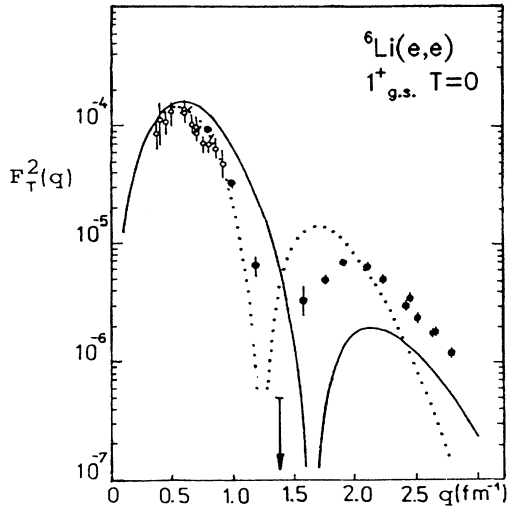


FIG. 8. Transverse form factor in elastic electron scattering by  ${}^6\text{Li}$ . Shell model (Ref. 24; dotted line) and cluster model (Ref. 18; full line) calculations. Experimental data are from Ref. 31, Lapikás *et al.* (open circles) and Bergstrom *et al.* (full circles).

data very well for  $0 \leq q \leq 1.0 \text{ fm}^{-1}$ , but the dip in  $F_T^2(q)$  occurs here at too small  $q$  in comparison with the experiment.

Both the parametrization (15) and the  $\Psi_{3^+,0}$  wave function based on the admixture coefficients  $a_i$  from Table I reproduce the longitudinal transition  $(1^+,0) \rightarrow (3^+,0)$  form factor<sup>32,33</sup> perfectly in the whole interval  $0.4 \leq q \leq 2.5 \text{ fm}^{-1}$ , where data exist.

If one assumes the states  $(1^+,0)$  and  $(3^+,0)$  to be pure  $p$ -shell configurations (shell model  $M$ ), the transverse form factor receives contributions from the spin part of  $E2$  and  $M3$  form factors only, since the convection current contributions vanish in such an approximation. The corresponding  $E2$  ( $J=2$ ) and  $M3$  ( $J=3$ ) form factors are simply related to reduced matrix elements (14), which have now a particularly simple form

$$M_{(3^+,0)(1^+,0)}^{J210}(q) = c_J (bq)^2 \exp \left[ -\frac{A-1}{A} \frac{b^2 q^2}{4} \right]. \quad (16)$$

Here,  $b = 2.03 \text{ fm}$  is the harmonic oscillator constant and  $c_2$  and  $c_3$  is proportional to the admixture of  $(p_{3/2}, p_{1/2})$  and  $(p_{3/2})^2$  configuration in the  ${}^6\text{Li}$  ground-state wave function, respectively. This is the reason why the  $M3$  transition would dominate in the inelastic transverse form factor.

As was pointed out in Ref. 34, there is experimental evidence that the  $(3^+,0)$  level is almost completely longitudinal, and therefore the  $(1^+,0) \rightarrow (3^+,0)$  transverse form factor has not been measured yet.

The electromagnetic properties of  ${}^6\text{Li}$  will be discussed in a forth-coming application of the  $\Delta$ -hole model to  $\pi$ - ${}^6\text{Li}$  scattering.<sup>35</sup>

## V. RESULTS AND DISCUSSION

### A. Comparison of experimental data with theoretical predictions

The experimental results for the vector analyzing power and the “normalized” cross sections for  $\pi^+$ - ${}^6\text{Li}$  scattering are listed in Tables III and IV. These data supplemented by cross sections from Antonuk *et al.*<sup>9</sup> at 100 MeV and from Zichy *et al.*<sup>8</sup> at 164 MeV are displayed in Figs. 9 and 10 together with theoretical predictions by Junker (isobar-hole model) and Mach (coupled-channel model).

Before comparing the experimental data with the theoretical predictions some general observations should be made. In contrast to our results for  ${}^{15}\text{N}$ , a large analyzing power is observed for elastic and inelastic scattering. The shape of the angular distributions of  $iT_{11}$  changes little between 100 and 164 MeV. Further, it is interesting to note that for elastic scattering  $iT_{11}$  passes through zero at angles corresponding approximately to the cross-section minima. For inelastic scattering on the other hand  $iT_{11}$  has its maximum value near the minima of the cross sections.

In Fig. 9 the cross section and  $iT_{11}$  data are compared to calculations by Junker (see Sec. IV A). In these calculations the cross sections of Antonuk *et al.*<sup>9</sup> (180 and 240

TABLE III.  $iT_{11}$  for  $\pi^+$ - ${}^6\text{Li}$  scattering.

$T_\pi$ (MeV)	$\pi^+$ - ${}^6\text{Li}$ (ground state)		$\pi^+$ - ${}^6\text{Li}$ ( $3^+, 2.19 \text{ MeV}$ )	
	$\theta_{c.m.}$	$iT_{11}$	$iT_{11}$	$iT_{11}$
100	57.0	$0.137 \pm 0.037$		$0.205 \pm 0.116$
	67.2	$0.020 \pm 0.041$		$0.291 \pm 0.140$
	77.3	$-0.048 \pm 0.056$		$0.338 \pm 0.074$
	87.4	$-0.219 \pm 0.044$		$0.280 \pm 0.075$
	97.4	$-0.222 \pm 0.046$		$0.240 \pm 0.087$
	107.3	$-0.194 \pm 0.058$		$0.096 \pm 0.091$
	117.2	$-0.262 \pm 0.063$		$0.114 \pm 0.071$
	126.9	$-0.353 \pm 0.078$		$0.140 \pm 0.056$
134	52.1	$0.052 \pm 0.024$		$0.122 \pm 0.064$
	62.4	$0.007 \pm 0.047$		$0.185 \pm 0.065$
	72.5	$-0.304 \pm 0.044$		$0.337 \pm 0.049$
	82.7	$-0.246 \pm 0.047$		$0.273 \pm 0.064$
	92.7	$-0.306 \pm 0.041$		$0.268 \pm 0.049$
	102.7	$-0.298 \pm 0.047$		$0.229 \pm 0.036$
	112.7	$-0.357 \pm 0.068$		$0.191 \pm 0.035$
	164	42.1	$0.051 \pm 0.016$	
52.4		$0.036 \pm 0.036$		$0.058 \pm 0.037$
62.8		$-0.075 \pm 0.082$		$0.131 \pm 0.038$
73.1		$-0.292 \pm 0.059$		$0.213 \pm 0.034$
83.4		$-0.242 \pm 0.032$		$0.242 \pm 0.034$
93.4		$-0.268 \pm 0.041$		$0.205 \pm 0.028$
103.4		$-0.234 \pm 0.048$		$0.194 \pm 0.023$
219		54.4	$0.105 \pm 0.096$	
	68.7	$0.205 \pm 0.054$		$0.002 \pm 0.050$
	82.9	$0.056 \pm 0.055$		$-0.047 \pm 0.061$

MeV) have been fitted with four parameters (complex central and spin-orbit potential in the spreading potential). At 100 MeV two more fitting parameters were required for the repulsive  $S$ -wave  $\rho^2$  term of the background amplitude  $T_0$ . Using parameters interpolated from those for 100, 180, and 240 MeV the cross sections at 134 and 219 MeV are well reproduced. Having satisfied this necessary condition, namely a good agreement with the cross sections,  $iT_{11}$  was predicted. In the

case of elastic scattering there are certainly discrepancies with the  $iT_{11}$  data, but their trend, in particular the change in sign between 164 and 219 MeV, is reproduced. In the case of inelastic scattering to the  $3^+$  state, the trend of the  $iT_{11}$  data is also reproduced rather well. There is an almost perfect agreement with the data close to the  $\Delta_{33}$  resonance ( $T_\pi=164$  MeV), while discrepancies occur below ( $T_\pi=100$  and 134 MeV) and above it ( $T_\pi=219$  MeV). For both the elastic and the inelastic

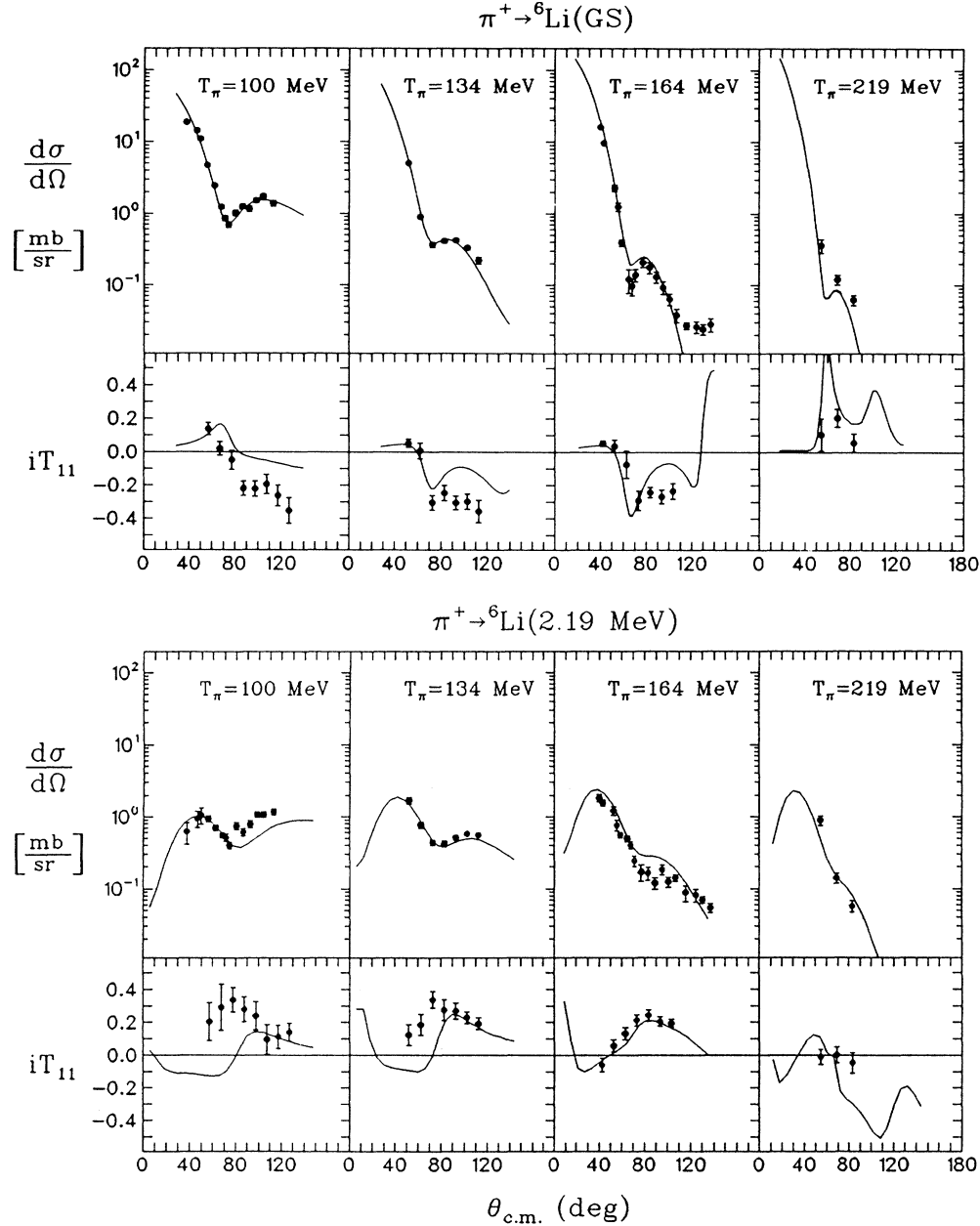


FIG. 9. Vector analyzing power  $iT_{11}$  for  $\pi^+ \text{-}^6\text{Li}$  (ground state) and  $\pi^+ \text{-}^6\text{Li}$  (2.19 MeV) scattering at 100, 134, 164, and 219 MeV, together with previously measured differential cross sections [Antonuk *et al.* (Ref. 9) at 100 MeV and Zichy (Ref. 8) at 164] and “normalized” cross sections from this experiment (at 134 and 219 MeV). The solid lines are the theoretical predictions of Junker “shell model  $J$ ” (see text).

scattering the predictions for  $iT_{11}$  show rapid changes in the angle which may be due to the wave function used. Particularly in the case of pion inelastic scattering leading to the  $(3^+, 0)$  state our nuclear structure input may be oversimplified. The admixture coefficients  $a_i$  in Eq. (11) are not determined uniquely by fitting just the C2 transition in  $(e, e')$  scattering. This is the reason why the spin structure of our  $(3^+, 0)$ -state wave function is not very reliable.

In Fig. 10 we compare the data with theoretical predictions by Mach. The solid and the dashed lines are calculations using shell models and cluster model wave functions, respectively, as described in Ref. 19 and Sec. IV B. For the excited state only the shell model wave function was available. For the elastic cross sections, there is reasonable agreement with the data except at  $T_\pi = 164$  MeV. Both wave functions produce almost identical results. This insensitivity to the nuclear structure input is

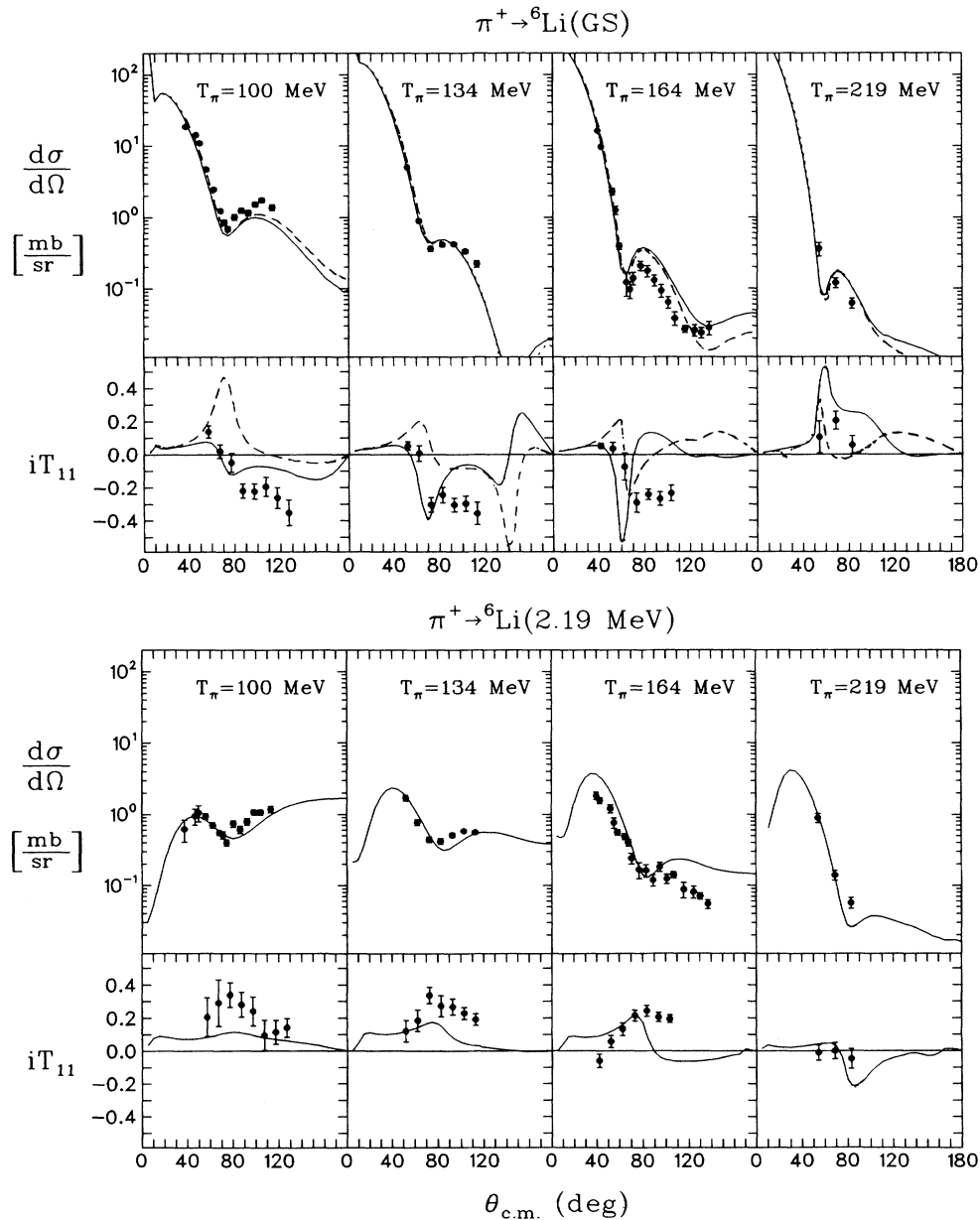


FIG. 10. The same data as shown in Fig. 9 compared with theoretical predictions from Mach. The solid lines correspond to shell model wave function "M", the dashed lines to cluster model wave function (see text).

TABLE IV.  $\pi^+{}^{-6}\text{Li}$  cross sections normalized to  $\pi^+{}-d$  cross sections from Ref. 27.

$T_\pi$ (MeV)	$\pi^+{}^{-6}\text{Li}$ (ground state)		$\pi^+{}^{-6}\text{Li}$ ( $3^+, 2.19$ MeV)
	$\theta_{\text{c.m.}}$	$d\sigma/d\Omega_{\text{c.m.}}$ (mb/sr)	$d\sigma/d\Omega_{\text{c.m.}}$ (mb/sr)
100	57.0	$2.658 \pm 0.163$	$0.745 \pm 0.176$
	67.2	$0.948 \pm 0.070$	$0.324 \pm 0.069$
	77.3	$0.469 \pm 0.043$	$0.435 \pm 0.047$
	87.4	$0.722 \pm 0.039$	$0.563 \pm 0.048$
	97.4	$1.012 \pm 0.052$	$0.790 \pm 0.074$
	107.3	$1.005 \pm 0.077$	$0.984 \pm 0.110$
	117.2	$0.906 \pm 0.084$	$1.161 \pm 0.124$
	126.9	$0.677 \pm 0.079$	$1.280 \pm 0.110$
134	52.1	$5.017 \pm 0.164$	$1.691 \pm 0.168$
	62.4	$0.886 \pm 0.061$	$0.772 \pm 0.072$
	72.5	$0.358 \pm 0.028$	$0.444 \pm 0.039$
	82.7	$0.410 \pm 0.029$	$0.416 \pm 0.040$
	92.7	$0.420 \pm 0.023$	$0.510 \pm 0.034$
	102.7	$0.331 \pm 0.021$	$0.578 \pm 0.028$
	112.5	$0.219 \pm 0.023$	$0.561 \pm 0.032$
	164	42.1	$11.558 \pm 0.575$
52.4		$1.895 \pm 0.161$	$1.993 \pm 0.177$
62.8		$0.231 \pm 0.039$	$0.711 \pm 0.060$
73.1		$0.178 \pm 0.020$	$0.388 \pm 0.025$
83.4		$0.267 \pm 0.016$	$0.342 \pm 0.022$
93.4		$0.177 \pm 0.014$	$0.342 \pm 0.019$
103.4		$0.105 \pm 0.010$	$0.296 \pm 0.013$
219		54.4	$0.341 \pm 0.074$
	68.7	$0.115 \pm 0.018$	$0.134 \pm 0.021$
	82.9	$0.060 \pm 0.009$	$0.054 \pm 0.009$

no longer observed for  $iT_{11}$ , where the two wave functions produce very different results, with a definite preference for the shell model. For the inelastic scattering the theoretical predictions are certainly in qualitative agreement with the trend of the cross-section and  $iT_{11}$  data.

As far as the pion elastic scattering is concerned, the predictions by Junker are in quite good agreement with the shell model calculations by Mach. Comparing the predictions from Junker (shell model  $J$ ) with those from Mach (shell model  $M$ ) one finds considerable similarity in the angular distribution of  $iT_{11}$ , in spite of the fact that the two reaction models are very different. This leads us once again to the conclusion that different reaction models may lead to similar predictions for  $iT_{11}$  provided that similar nuclear wave functions are used.

#### B. Analysis of $iT_{11}$ in terms of nuclear form factors and $\pi N$ amplitudes

Recently, the vector analyzing power in pion *elastic* scattering by polarized  $p$ -shell nuclei has been analyzed by Mach and Kamalov<sup>36</sup> in terms of nuclear form factors and elementary  $\pi N$  amplitudes. Here we extend such an analysis to the case of pion *inelastic* scattering by polarized nuclei. Using the distorted-wave impulse approxi-

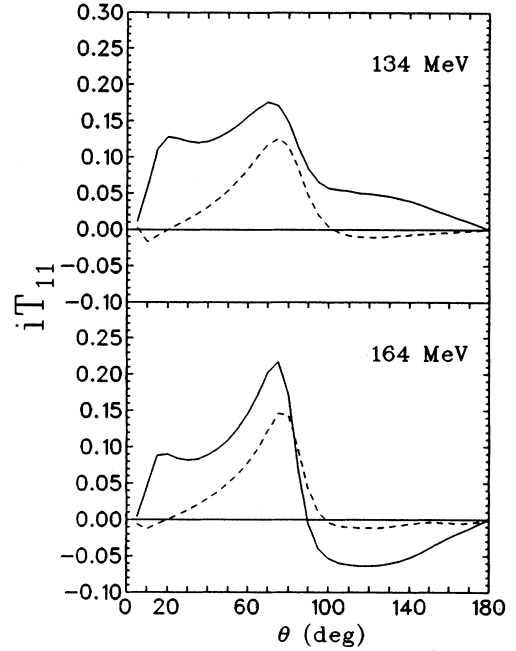


FIG. 11. Vector analyzing power  $iT_{11}$  for  $\pi^+{}^{-6}\text{Li}$  (2.19 MeV) scattering. The solid lines correspond to the coupled channel calculation, the dashed lines denote the PWIA results.

mation (DWIA), we can write the pion-nucleus amplitude in the form

$$\langle f|T|i\rangle = A \langle \phi_{\text{dist}}^{(-)} | \langle \Psi_{\text{nucl}}^f | V_0 + i\sigma \mathbf{v} V_1 | \Psi_{\text{nucl}}^i \rangle | \phi_{\text{dist}}^{(+)} \rangle, \quad (17)$$

where  $\mathbf{v}$  is the unit vector perpendicular to the scattering plane and  $V_0$  and  $V_1$  are the scalar and spin-flip parts of the  $\pi N$  amplitude, respectively. Since the nucleon spin operator is averaged in Eq. (17) between nuclear states and the matrix elements  $\langle \Psi_{\text{nucl}}^f | \sigma | \Psi_{\text{nucl}}^i \rangle$  receive contributions from valence nucleons only, one can expect large sensitivity of  $iT_{11}$  to the nuclear structure input, particularly to spin distributions in nuclei.

A quite different situation occurs in inelastic scattering of polarized protons by unpolarized nuclei. Equation (17) is also applicable there ( $V_0$  and  $V_1$  have different meaning), however the spin matrix elements  $\langle \phi_{\text{dist}}^{(-)} | \sigma | \phi_{\text{dist}}^{(+)} \rangle$  enter Eq. (17) in such a case. Therefore,  $iT_{11}$  in  $\bar{p}-A$  inelastic scattering is very sensitive to the distortion in initial and final state.

In Fig. 11 we show the role of the distortion effects in  $\pi^+{}^{-6}\text{Li}$  inelastic scattering at two energies. A comparison is made between  $iT_{11}$  calculated using the coupled-channel (CC) approach and plane-wave impulse approximation (PWIA), i.e., neglecting completely the distortion in initial and final state. Apart from the region of small scattering angles the two results are quite similar. Particularly, CC and PWIA predict the peak in  $iT_{11}$  at approximately the same angle.

Since the shape of  $iT_{11}$  in  $\pi^{-6}\text{Li}$  scattering is not determined by distortion effects, it is meaningful to use the PWIA for discussing gross features of the vector analyzing power. In the case of the  $(1^+, 0) \rightarrow (3^+, 0)$  transition we have

$$iT_{11} = \frac{1}{\sqrt{2}} \frac{\text{Im}(V_0^* V_1) M_{\text{in}}^{2200}(q) [M_{\text{in}}^{2210}(q) + (4\sqrt{2}/7) M_{\text{in}}^{3210}(q)]}{|V_0|^2 M_{\text{in}}^{2200}(q)^2 + \frac{1}{2} |V_1|^2 [M_{\text{in}}^{2210}(q)^2 + \frac{4}{7} M_{\text{in}}^{3210}(q)^2]}, \quad (18)$$

where  $M_{\text{in}}^{JLST}(q) \equiv M_{(3^+,0)(1^+,0)}^{JLST}(q)$  are defined in Eq. (14). If we suppose the  $(1^+,0)$  and  $(3^+,0)$  states to be pure  $p$ -shell configurations,  $M_{\text{in}}^{2200}(q)$  has the same simple form (16) as the spin form factors and the  $q$ -dependent part of nuclear input cancels out in Eq. (18). Since  $c_2$  and  $c_3$  in Eq. (16) have the same sign, the  $E2$  and  $M3$  matrix elements add constructively in Eq. (18). We can conclude that the angular distribution of  $iT_{11}$  is determined in this case by the isoscalar combinations of  $\pi N$  amplitudes  $V_0$  and  $V_1$ . The same amplitudes determine  $iT_{11}$  in  $\pi^+d$  scattering. Therefore, similarity of  $iT_{11}$  in  $\pi^+d$  elastic and  $\pi^{+6}\text{Li}$  inelastic  $(1^+,0) \rightarrow (3^+,0)$  reaction is not surprising.

The situation in  $\pi^{+6}\text{Li}$  elastic scattering is quite different. Here we have

$$iT_{11} = \sqrt{2/3} \frac{\text{Im}(V_0^* V_1) [M_{\text{el}}^{0000}(q) - \frac{q^2}{2\sqrt{2}} M_{\text{el}}^{2200}(q)] F_{\text{el}}^S(q)}{|V_0|^2 (M_{\text{el}}^{0000}(q)^2 + q^2 M_{\text{el}}^{2200}(q)^2) + |V_1|^2 F_{\text{el}}^S(q)^2 / 3} \quad (19)$$

in PWIA approach. Further,

$$F_{\text{el}}^S(q) = M_{\text{el}}^{1010}(q) - \frac{q^2}{\sqrt{2}} M_{\text{el}}^{1210}(q) \quad (20)$$

and  $M_{\text{el}}^{JLST}(q) \equiv M_{(1^+,0)(1^+,0)}^{JLST}(q)$  are defined again in Eq. (14). Recently, it has been shown<sup>36</sup> that the shape of  $iT_{11}$  in pion elastic scattering by  $p$ -shell nuclei is influenced to large extent by the shape of the spin form factor  $F_{\text{el}}^S(q)$ . In particular, the leftmost zero of  $iT_{11}$  is associated in the resonance region with the zero of the spin form factor Eq. (20). We can conclude that the different shapes of the angular distributions of  $iT_{11}$  in the elastic scattering and the inelastic  $(1^+,0) \rightarrow (3^+,0)$  transition are caused mainly by the very different shapes of the corresponding nuclear spin form factors.

### C. Sensitivity of $iT_{11}$ to nuclear structure input and reaction formalism

Regarding the question of the sensitivity of the polarization observable  $iT_{11}$  to the reaction model and the nuclear wave function we show in Fig. 12 the cross sections of Antonuk *et al.*,<sup>9</sup> our normalized cross sections from this experiment, and the vector analyzing power, together with the predictions from the four theory groups mentioned in the introduction. Germond<sup>17</sup> (solid line), Eramzhyan<sup>19</sup> (dot-dashed line), and Nagaoka and Ohta<sup>21</sup> (dotted line), all used the  $\alpha$ - $n$ - $p$  three body cluster wave function of Krasnopol'ski *et al.*<sup>18</sup> Mach (dot-long-dashed line) and Junker (dashed line) on the other hand used shell model wave functions in the calculations shown. With the exception of Junker (who fit the data of Antonuk<sup>9</sup> to determine the parameters of the spreading potential) all cross section predictions agree more or less among each other, and with our "normalized" cross sections. This remarkable agreement shows how insensitive cross sections are to the scattering model and to the nuclear structure input. The vector analyzing power  $iT_{11}$  on the other hand, appears to be sensitive mostly to the nuclear structure. The scattering models of Germond<sup>17</sup> (Glauber model) and Eramzhyan *et al.*<sup>19</sup> (momentum space coupled channel calculation) produce identical results, and the prediction of Nagaoka and Ohta<sup>21</sup> ( $\Delta$ -hole model) is

not far away. On the other hand, quite different results are obtained by Mach and Junker with shell model wave functions. They come closer to the data. Also note, that the differences between the various predictions for  $iT_{11}$  are largest at angles close to the minimum of the cross section, indicating delicate interferences between the spin-flip and non-spin-flip amplitudes.

From the discussion in the previous section and in Ref. 36 it follows that the shape of  $iT_{11}$  in pion elastic scattering from  ${}^6\text{Li}$  is strongly influenced by the shape of nuclear spin form factor. The form factor  $F_{\text{el}}^S(q)$  is not

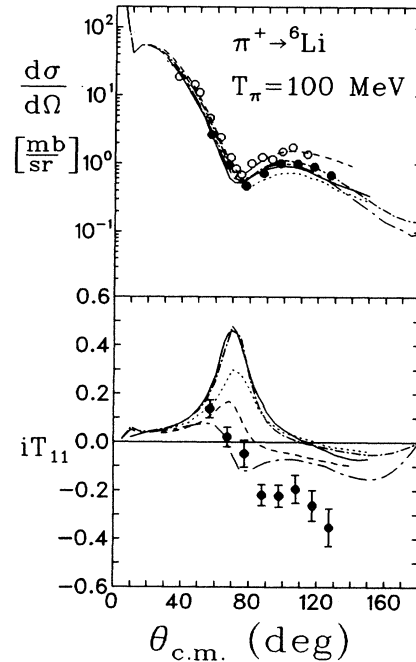


FIG. 12. Vector analyzing power  $iT_{11}$  and "normalized" cross sections from this experiment (solid circles); cross sections from Antonuk *et al.* (Ref. 9; open circles). The five curves are theoretical predictions from Germond (Ref. 17; solid line), Eramzhyan (Ref. 19; dot-short-dashed line) Nagaoka and Ohta (Ref. 21; dotted line), all using the cluster wave function from Ref. 18. Junker (dashed line) and Mach (dot-long-dashed line), both using shell model wave functions. Note the remarkable sensitivity of the predictions for  $iT_{11}$  to the nuclear wave function in the region of the minima of the cross section.

directly accessible in electron scattering experiments. However, the transversal form factor  $F_T$  is expected to be very close to  $F_{cl}^S(q)$  because the convection current contribution almost vanishes in  $e^{-6}\text{Li}$  scattering, if  $L=0$  is really the dominating configuration in the  ${}^6\text{Li}$  ground-state wave function. We recall once again Fig. 8, where experimental data for  $F_T(q)$  are shown along with the cluster model (solid line) and shell model (dotted line) predictions and remind the reader that the nuclear wave functions used in our isobar-hole and coupled-channel calculations (shell model version) lead to exactly the same  $F_T(q)$  (dotted line). It is interesting to note that the zero of  $F_T(q)$  as obtained from the shell model,  $q=1.3\text{ fm}^{-1}$ , occurs at too low a momentum transfer in comparison with the experiment ( $q=1.4\text{ fm}^{-1}$ ). At the same time, the first zero of  $iT_{11}$  as predicted by both the isobar-hole and coupled-channel models (shell model version) also occurs at scattering angles which are too low in comparison with experiment. This can clearly be seen at  $T_\pi=134$  and  $164\text{ MeV}$ . On the other hand, the cluster model wave function produces a zero of  $F_T(q)$  at too large  $q$ :  $q\cong 1.6\text{ fm}^{-1}$ . The coupled-channel calculations (cluster model version) for  $iT_{11}$  change sign at scattering angles which are too large (see Fig. 10) in comparison with the experiments. In fact the main reason why the cluster and shell model predict such different  $iT_{11}$  in  $\pi^{-6}\text{Li}$  elastic scattering is the different shape of the spin form factor  $F_{cl}^S(q)$  obtained using the two models.

In order to see whether a better representation of the

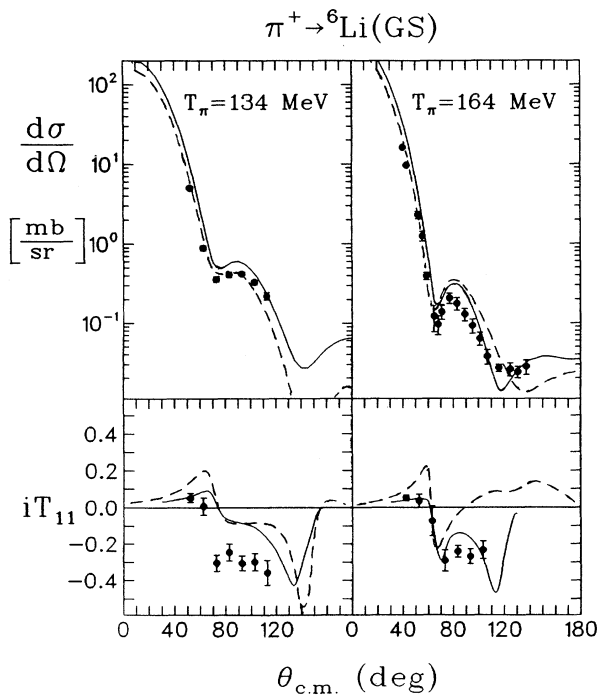


FIG. 13. Effects of the second-order potential in the calculation by Mach using the cluster wave function. The solid curve is the prediction with the first order potential only, the dashed curve is the full calculation with the second-order potential included. The data are the same as shown in Fig. 9 and Fig. 10.

transverse form factor may improve the theoretical predictions for  $iT_{11}$  a phenomenological transition density which fitted the elastic transverse form factor was used in the coupled-channel calculation (shell model  $M$ ). As one may have suspected the resulting angular distribution of  $iT_{11}$  was found to be between the ones for the cluster and the shell model wave functions, but closer to the cluster wave function. This means worse agreement with the experiment. These observations strongly indicate the necessity of using reliable wave functions in predicting spin observables in pion nucleus scattering.

Having shown the sensitivity of  $d\sigma/d\Omega$  and  $iT_{11}$  to the nuclear wave function, we would also like to give an example of their sensitivity to modifications of the scattering model. In Fig. 13 we compare the predictions for  $d\sigma/d\Omega$  and  $iT_{11}$  from Mach for the full calculation (dashed line) with the calculations when the 2nd order potential is turned off (solid line). In both cases, the clus-

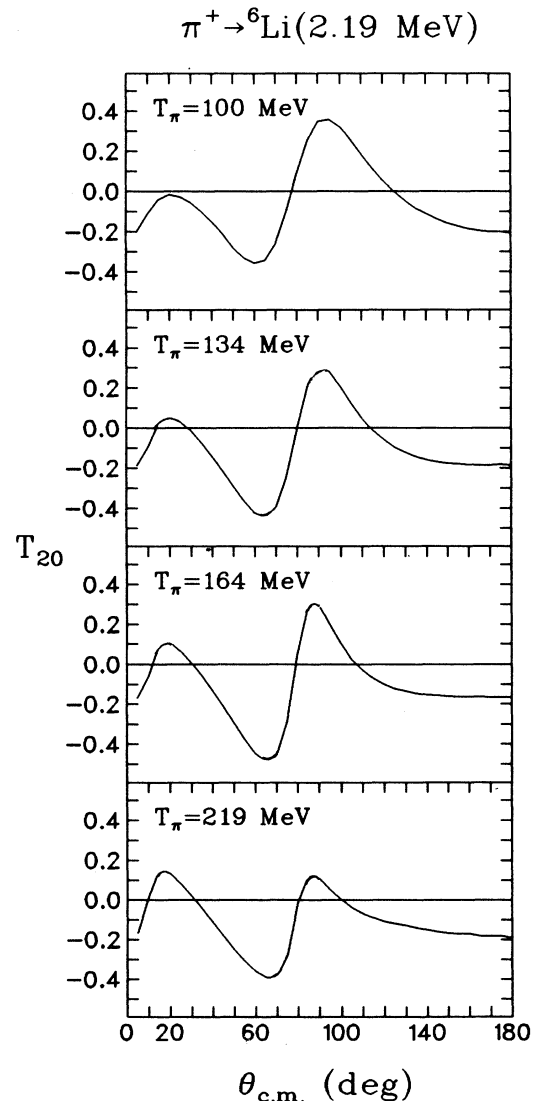


FIG. 14. Theoretical prediction for  $T_{20}$  in the coupled-channel model by Mach for  $\pi^{+6}\text{Li}$  scattering to the  $3^+$ , 2.19 MeV state.

ter model wave function was used. The data are the same as shown in Figs. 9 and 10.

At forward angles, the cross-section data favor the inclusion of the second-order potential. For  $iT_{11}$  we see little differences between the first- and second-order models at 134 MeV, but large differences at 164 MeV. This strong energy dependence is quite surprising and not yet understood.

## V. CONCLUSIONS AND OUTLOOK

After the striking result which we have obtained for the asymmetry  $A_y$  in  $\pi^+$ - $^{15}\text{N}$  scattering, the first data on the vector analyzing power  $iT_{11}$  in  $\pi^+$ - $^6\text{Li}$  scattering also show remarkable discrepancies from theoretical predictions. From the comparison of calculations using different scattering models and/or different wave functions for  $^6\text{Li}$  it already appears that the vector analyzing power  $iT_{11}$  will give more information on the nuclear wave function than on the scattering formalism, although it cannot be ruled out that by fine tuning the scattering theory, in conjunction with more extensive data on several polarization observables, new information may be also obtained on details of the scattering models.

Since we are just at the beginning of this research program there are many interesting aspects for further  $\pi^+$ - $^6\text{Li}$  studies. The present measurements of the vector analyzing power  $iT_{11}$  must be extended in the angular and energy range. Also, large values for the tensor analyzing power  $T_{20}$  for the  $3^+$ , 2.19 MeV state are predicted by the  $\Delta$ -hole model and the coupled-channel model. Prediction from the latter one are shown in Fig. 14. This observable should be explored. In addition, the spin dependence in the most important pion induced reaction channels should be investigated in kinematically complete experiments. Similar studies of spin dependence are in progress at LAMPF and TRIUMF for the nuclei  $^7\text{Li}$  and  $^{13}\text{C}$ . Such systematic measurements will finally provide a better understanding of the spin dependence in pion nuclear interactions.

## ACKNOWLEDGMENTS

This work would have been impossible without the generous help and considerable skills of the staff of the Paul Scherrer Institute. It has been funded by the German Federal Minister for Research and Technology (BMFT) under the Contract No. 06 KA 265.

\*Present address: Department of Physics, University of Regina, Regina, Saskatchewan, Canada S4S 0A2.

<sup>1</sup>R. Tacik *et al.*, Phys. Rev. Lett. **63**, 1784 (1989).

<sup>2</sup>R. Meier *et al.*, Phys. Rev. C **42**, 2222 (1990).

<sup>3</sup>A. Abragam, in *High Energy Physics with Polarized Beams and Polarized Targets (Argonne, 1978)*, Proceedings of the Third International Symposium, AIP Conf. Proc. No. 51, edited by G. H. Thomas (AIP, New York, 1979).

<sup>4</sup>V. Bouffard, Y. Roinel, P. Roubeau, and A. Abragam, J. Phys. (Paris) **41**, 1447 (1980).

<sup>5</sup>P. Chaumette, J. Deregel, G. Durand, J. Fabre, J. Morchet, and J. Ball, Proceedings of the 4th International Workshop on Polarized Target Materials and Techniques, Bad Honnef, Germany, 1984, edited by W. Meyer [University of Bonn report (unpublished)], p. 81.

<sup>6</sup>P. Chaumette, J. Deregel, G. Durand, J. Fabre, and L. van Rossum, in *High Energy Spin Physics*, Proceedings of the Eighth International Symposium, Minneapolis, 1988, edited by K. J. Heller, AIP Conference Proceeding (AIP, New York, 1989), Vol. 2, p. 1275.

<sup>7</sup>F. Ajzenberg-Selove, Nucl. Phys. **A413**, 1 (1984). For more recent work on nucleon and electron scattering off  $^6\text{Li}$  see C. W. Glover *et al.* Phys. Rev. C **41**, 2487 (1990), and V. I. Kukulin, V. T. Voronchev, T. D. Kaipov, and R. A. Eramzhyan, Nucl. Phys. **A517**, 221 (1990).

<sup>8</sup>J. Zichy, Ph.D. thesis No. 6612 ETH Zürich, 1980.

<sup>9</sup>L. E. Antonuk *et al.*, Nucl. Phys. **A451**, 741 (1986).

<sup>10</sup>R. R. Kiziah *et al.*, Phys. Rev. C **30**, 1643 (1984).

<sup>11</sup>R. D. McKeown, S. J. Sanders, J. P. Schiffer, H. E. Jackson, M. Paul, J. R. Specht, E. F. Stephenson, R. P. Redwine, and R. E. Segel, Phys. Rev. C **24**, 211 (1981).

<sup>12</sup>D. Renker *et al.*, Phys. Rev. Lett. **41**, 1279 (1978).

<sup>13</sup>F. Calligaris, C. Cernigoi, I. Gabrielli, and F. Pellegrini, Nucl. Phys. **A126**, 209 (1969); B. Bassaleck, E. L. Haase, W. D.

Klotz, F. Takeutchi, H. Ullrich, M. Furič, and Y. Sakamoto, Phys. Rev. C **19**, 1893 (1979); H. P. Isaak, P. Heus, H. S. Pruyss, R. Engfer, E. A. Hermes, T. Kozłowski, U. Sennhauser, and H. K. Walter, Helv. Phys. Acta **55**, 477 (1982).

<sup>14</sup>R. L. Burman and M. E. Nordberg, Phys. Rev. Lett. **165**, 1096 (1968); N. Favier, T. Bressani, G. Charpak, L. Massonet, W. E. Meyerhof, and Č. Zupančič, Nucl. Phys. **A169**, 540 (1971); E. D. Arthur *et al.*, Phys. Rev. C **11**, 332 (1975); R. Rieder *et al.*, *ibid.* **33**, 614 (1986); Z. Zhang *et al.*, Bull. Am. Phys. Soc. **33**, 1586 (1988).

<sup>15</sup>J. D. Hurd, J. S. Boswell, R. C. Minehart, Y. Tzeng, H. J. Ziocck, K. O. H. Ziocck, L. C. Liu, and E. R. Siciliano, Nucl. Phys. **A475**, 743 (1987).

<sup>16</sup>G. J. Lolos, R. R. Johnson, P. Couvert, J. McKenna, R. Myers, I. Spadinger, and P. Lorraine, Phys. Lett. **126B**, 20 (1983); P. D. Barnes *et al.*, Nucl. Phys. **A402**, 397 (1983); B. J. McParkland *et al.*, Phys. Lett. **156B**, 47 (1985); B. J. McParkland *et al.*, Nucl. Phys. **A456**, 629 (1986).

<sup>17</sup>J. F. Germond, J. Phys. G **12**, 609 (1984).

<sup>18</sup>V. M. Krasnopol'ski, V. I. Kukulin, P. B. Sazonov, and V. T. Voronchev, Phys. Lett. **121B**, 96 (1983); Nucl. Phys. **A417**, 128 (1984).

<sup>19</sup>R. A. Eramzhyan, M. Gmitro, T. D. Kaipov, S. S. Kamalov, and R. Mach, J. Phys. G **14**, 1511 (1988).

<sup>20</sup>K. Junker (unpublished).

<sup>21</sup>R. Nagaoka and K. Ohta, Ann. Phys. (N.Y.) **84**, 148 (1988).

<sup>22</sup>M. Hirata, F. Lenz, and K. Yazaki, Ann. Phys. (N.Y.) **108**, 116 (1977).

<sup>23</sup>Y. Horikawa, M. Thies, and F. Lenz, Nucl. Phys. **A345**, 386 (1980).

<sup>24</sup>T. W. Donnelly and J. D. Walecka, Phys. Lett. **44B**, 330 (1973).

<sup>25</sup>V. König and W. Grüberler, Nucl. Phys. **A148**, 380 (1970).

<sup>26</sup>C. R. Ottermann *et al.*, Phys. Rev. C **38**, 2310 (1988).

- <sup>27</sup>K. Gabathuler *et al.*, Nucl. Phys. **A350**, 253 (1980).
- <sup>28</sup>M. Wessler *et al.*, Nucl. Instrum. Methods (to be published).
- <sup>29</sup>E. Ferreira and H. G. Dosch, Phys. Rev. C **40**, 1750 (1989).
- <sup>30</sup>M. Gmitro, S. S. Kamalov, and R. Mach, Phys. Rev. C **36**, 1105 (1987).
- <sup>31</sup>R. E. Rand, R. Frosch, and M. R. Yearian, Phys. Rev. **144**, 1859 (1966); L. Lapikás, in Proceedings of the Conference on Modern Trends in Elastic Electron Scattering, Amsterdam, 1978 (unpublished); J. C. Bergstrom, S. B. Kowalski, and R. Neuhausen, Phys. Rev. C **25**, 1156 (1982).
- <sup>32</sup>R. Yen, L. S. Cardman, D. Kalinsky, J. R. Legg, and C. K. Bockelman, Nucl. Phys. **A235**, 135 (1974).
- <sup>33</sup>J. C. Bergstrom, N. Deutschmann, and R. Neuhausen, Nucl. Phys. **A327**, 439 (1979).
- <sup>34</sup>G. C. Li, I. Sick, R. R. Whitney, and M. R. Yearian, Nucl. Phys. **A162**, 583 (1971).
- <sup>35</sup>K. Junker (unpublished).
- <sup>36</sup>R. Mach and S. S. Kamalov, Nucl. Phys. **A551**, 601 (1990).